



Transition sandwich Janus membrane of cellulose acetate and polyurethane nanofibers for oil–water separation

Yong Zhang · Mei Yang · Yuan Zhou · Anrong Yao · Yanting Han ·
Yidong Shi · Fei Cheng · Mi Zhou · Puxin Zhu · Lin Tan

Received: 16 September 2021 / Accepted: 23 December 2021 / Published online: 4 January 2022
© The Author(s), under exclusive licence to Springer Nature B.V. 2022

Abstract Through sequential electrospinning, a sandwich Janus membrane (PU-(CA/PU)-CA) was constructed with hydrophobic polyurethane (PU) nanofiber membrane as the top layer, cellulose acetate/polyurethane (CA/PU) blend nanofiber membrane as the intermediate transition layer and hydrophilic cellulose acetate (CA) nanofiber membrane as the bottom layer. The effects of membrane structure, composition and thickness on the mechanical properties, permeability and separation ability of PU-(CA/PU)-CA nanofiber membrane were studied. The results show that the transition sandwich structure PU-(CA/PU)-CA membrane has good mechanical properties, high permeability and selective separation ability, and can realize the unidirectional transmission

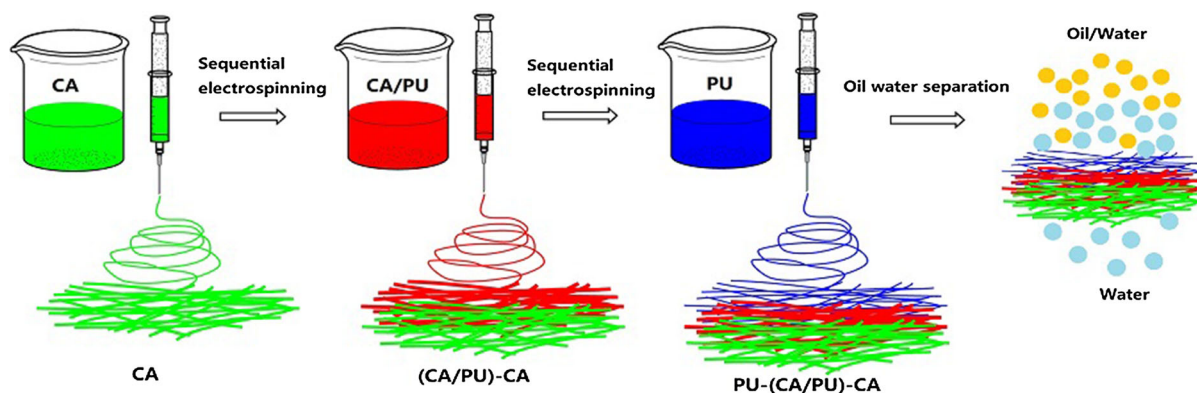
of water and efficient oil–water separation. When the membrane thickness is 80 μm , the hydraulic permeability is $3.4 \pm 0.4 \times 10^4 \text{ L}/(\text{m}^2 \text{ h bar})$, the oil–water separation efficiency reaches $99 \pm 0.4\%$, and the tensile strength is 95.8% higher than that of the double-layer PU-CA membrane. The thermal stability and antifouling ability of PU-(CA/PU)-CA nanofiber membrane have also been improved, and the reusability is good. CA/PU transition interlayer improves the interfacial compatibility between CA and PU nanofiber membrane, enhances the performance of PU-(CA/PU)-CA nanofiber Janus membrane, and shows its application prospect in the field of separation and purification.

Supplementary Information The online version contains supplementary material available at <https://doi.org/10.1007/s10570-021-04402-8>.

Y. Zhang · Y. Zhou · A. Yao · Y. Han ·
Y. Shi · F. Cheng · M. Zhou · P. Zhu · L. Tan (✉)
College of Biomass Science and Engineering, Sichuan
University, Chengdu 610065, China
e-mail: scuzhang@scu.edu.cn; tanlinou@scu.edu.cn

M. Yang
College of Physics and Technology Engineering, Chengdu
Normal University, Chengdu 611130, China

Graphical abstract



Keywords Cellulose acetate · Polyurethane · Nanofibers · Transition sandwich structure · Janus membrane

Introduction

Electrospun nanofiber membrane has the advantages of high specific surface area, good flexibility, adjustable wettability, high porosity and good pore connectivity. It can separate oil–water mixture with high permeability and low energy consumption. It has attracted more and more attention in the field of wastewater treatment (Zhang, et al. 2019a, b; Su et al. 2021; Cárdenas Bates et al. 2021). However, it is difficult for single polymer and single-layer nanofiber membranes to obtain the best mechanical strength, permeability and selective separation ability at the same time (Cui et al. 2020; Wang et al. 2016a, b). Therefore, it is necessary to construct multilayer nanofiber membranes with special structure and properties to overcome this limitation (Ju et al. 2021; Dai et al. 2020).

Janus membrane refers to the membrane with asymmetric properties on both sides, and its asymmetric properties come from different membrane materials and/or membrane structures. The difference in wettability on both sides of Janus membrane will lead to unique transport behavior in the membrane (Yang et al. 2016), such as unidirectional liquid infiltration (Song et al. 2019; Liu et al. 2019, 2017; Xie et al. 2021; Wu et al. 2012) and oil–water separation

(Wang et al. 2016a, b; Li et al. 2019). This makes Janus membrane have a unique position in the field of separation and purification. Janus membranes can be obtained by a simple sequential stacking method. For example, Janus filter membranes are prepared by sequentially filtering hydrophilic and hydrophobic nanotubes or nanowires onto porous substrates (Zhang et al. 2014; Hu et al. 2015), or Janus nanofiber membranes are prepared by sequential electrospinning of hydrophilic and hydrophobic polymers (Wu et al. 2012). The sequential superposition method can easily control the thickness of each layer of membrane material, and consequently adjust the filtration and separation capacity of the membrane. However, in order to ensure the mechanical strength of the prepared Janus membrane, the interfacial compatibility between two adjacent membrane materials must be considered (Yang et al. 2016).

At present, a variety of polymers can be used for electrospinning to prepare nanofiber membranes. Among them, CA is one of the commonly used membrane materials. It has good biocompatibility, good hydrophilicity, fouling resistance and chlorine resistance. Its disadvantages are poor mechanical strength and low chemical resistance (Yao et al. 2021; Zhang et al. 2021; Jiang et al. 2020; Nosar et al. 2016). PU is a copolymer formed by alternating arrangement of soft and hard chain segments, which has unique mechanical properties, such as higher tensile strength, flexibility and ability to withstand extreme temperature conditions, which makes PU competitive in many industrial membrane separation applications (Zavastin et al. 2010; Riaz et al. 2016).

PU is not only different from CA in wettability, but also can make up for the deficiency of CA in mechanical strength. Based on this, we constructed a Janus membrane (PU-(CA/PU)-CA) with transition sandwich structure composed of CA and PU nanofibers by sequential electrospinning. The top layer of PU-(CA/PU)-CA membrane is PU nanofibers, the bottom layer is CA nanofibers, and the middle transition layer is CA/PU blend nanofibers. The top layer (hydrophobic) and bottom layer (hydrophilic) of this Janus membrane have different wetting properties, which is expected to realize the functions of water directional transmission and oil–water separation. The transition interlayer increases the compatibility between the top layer and the bottom layer, and can enhance the mechanical properties of the membrane. The properties of PU-(CA/PU)-CA nanofiber membrane were systematically characterized by infrared spectroscopy, thermogravimetric analysis, scanning electron microscopy, filtration experiment and tensile test. The contact angle, hydraulic permeability, oil–water separation efficiency and mechanical properties of the membrane were measured. The effects of membrane composition and structure on permeability, oil–water separation ability and mechanical properties were studied.

Experiments

Materials

Cellulose acetate (degree of substitution 2.4) was provided by Sichuan Push Acetate Co., Ltd. Polyurethane (3390ARE), purchased from Shanghai Hiend polyurethane company, is a block polyether polyurethane with butanediol (BDO) as chain extender and diphenylmethane diisocyanate (MDI) and polyethylene glycol (PEG) as raw materials (Fig. S1). The average molecular weight of soft segment PEG is 1000 Da. Methyl blue, 4-aminoazobenzene, n-hexane, cyclohexane, petroleum ether, N, N-Dimethylacetamide (DMAc) and acetone were obtained from Chengdu Kelong Chemical Co., Ltd. Sunflower vegetable oil was purchased from Wal Mart supermarket. All materials are used directly without further purification.

Preparation of nanofiber membrane

The preparation diagram of PU-(CA/PU)-CA nanofiber transition sandwich Janus membrane is shown in Fig. 1. Firstly, 10 g CA was dissolved in 90 g acetone-DMAc (2:1, w/w) mixed solution to obtain 10 wt% CA spinning solution. 10 g PU was dissolved in 90 g DMAc to obtain 10 wt% PU spinning solution. 5 g CA and 5 g PU were dissolved in 90 g acetone-DMAc (2:1, w/w) mixed solution to obtain CA/PU blended spinning solution. Electrospinning was carried out successively with PU, CA/PU and CA spinning solution at room temperature, voltage of 1.4–1.6 kV/cm, relative humidity of $50 \pm 5\%$ and spinning solution feeding speed of 1.0 mL/h. The thickness ratio of PU layer, CA/PU layer and CA layer is 2:1:2. The thickness and thickness ratio of each layer are controlled by controlling the spinning time, and PU-(CA/PU)-CA nanofiber Janus membranes (Fig. S2) with total thickness of 50, 80, 120 and 150 μm are obtained, which are recorded as M_{50} , M_{80} , M_{120} and M_{150} respectively. Under the same electrospinning conditions, pure CA membrane, pure PU membrane and CA/PU blend nanofiber membrane were prepared as control. In order to compare the effects of membrane structure on the mechanical properties and separation properties of the membrane, PU and CA spinning solution were electrospun successively to obtain PU-CA bilayer Janus membrane with a thickness ratio of PU layer to CA layer of 1:1 as the control.

Characterization

Fourier transform infrared spectroscopy (FTIR) analysis of the membranes was performed by using Tracer-100 infrared spectrum scanner (Shimadzu, Japan) with a range of $4000\text{--}600\text{ cm}^{-1}$ and a resolution of 4 cm^{-1} .

TG 209 F3 thermal analyzer (Netzsch, Germany) was used for thermogravimetric (TG) analysis of the membranes. The heating rate was $10\text{ }^\circ\text{C}/\text{min}$ and the relative mass loss of the membrane samples (3–5 mg) was recorded between 30 and $600\text{ }^\circ\text{C}$.

The morphology of the membranes surface before and after used was observed by Nova Nano SEM 450 field emission scanning electron microscope (SEM) (FEI, USA), and the fracture surface after the membranes were brittle fractured in liquid nitrogen was observed.

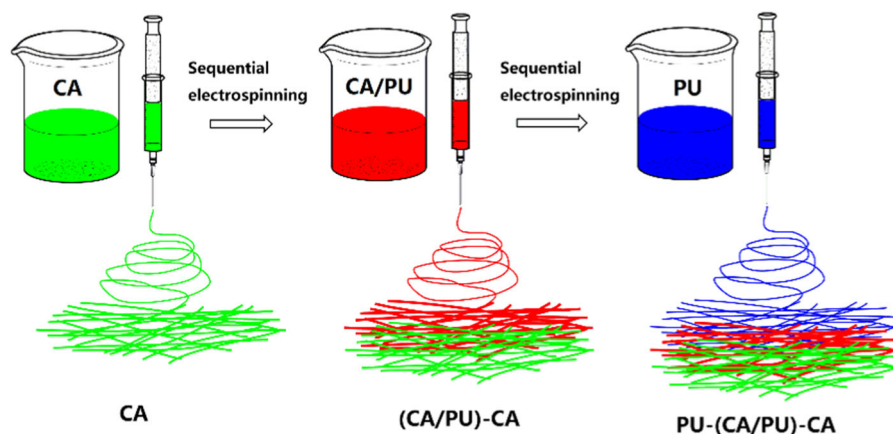


Fig. 1 Schematic diagram of PU-(CA/PU)-CA nanofiber transition sandwich Janus membrane prepared by electrospinning

The water and oil contact angle of the membranes were measured with DSA25 goniometer (KRUSS, Germany) and the average of 5 measurements was taken.

Jinteng 250 sand core filter and SHB-3 water circulation multi-function vacuum pump (Beijing Keweyongxing, China) were used for filtration experiment at 25 °C. The filtration area of nanofiber membrane was 3.14 cm², and each experiment was repeated five times. Firstly, the prepared nanofiber membrane is fixed on the sand core filter, and then the sand core filter is connected with self-made capillary tee pressure regulator and the vacuum pump. The oil water mixture to be separated is poured into the funnel of the sand core filter, and the vacuum pump is turned on. The transmembrane pressure, filtration volume and filtration time are recorded. The membrane hydraulic permeability (L_p) is calculated by the following expression (Yao et al. 2021):

$$L_p = \frac{v}{S \cdot t \cdot \Delta p} \quad (1)$$

where S is the filtration area of membrane, t stands for the duration of the collection of the permeate, Δp is the transmembrane pressure and V represents the volume of permeate collected during the time interval t .

The oil–water separation efficiency was determined by the weight ratio of the oil intercepted on the membrane after separation to the oil in the oil–water mixture before separation, and each test was repeated 5 times. The calculation formula is as follows (Liu et al. 2018; Zhang et al. 2017):

$$E_s(\%) = \frac{m}{m_0} \times 100 \quad (2)$$

where m_0 is the weight of oil in the oil–water mixture before separation and m is the weight of oil retained on the membrane after separation.

Tensile tests were carried out on 5967 universal testing machine (Instron, USA) with a load capacity of 1 kN and a stretching speed of 5 mm/min at room temperature and humidity 60%. The mean value of 5 parallel measurements for each membrane was calculated.

Results and discussion

Infrared spectroscopy and thermogravimetric analysis

FTIR is mainly used to analyze the structure and functional groups of polymer main chain. The FTIR spectra of pure PU and pure CA nanofiber membranes and CA/PU blend nanofiber membrane are shown in Fig. 2a. The absorption peaks at 2944 and 1433 cm⁻¹ are the asymmetric tensile vibration peak and bending vibration peak of CH₂ respectively, and the absorption peak at 1730 cm⁻¹ is the carbonyl C=O stretching vibration peak. These absorption peaks are characteristic peaks of the same functional groups of CA and PU. The absorption peak at 3334 cm⁻¹ is caused by the stretching vibration of N–H, and the absorption peak at 1528 cm⁻¹ belongs to the bending vibration of N–H. These absorption peaks are the characteristic

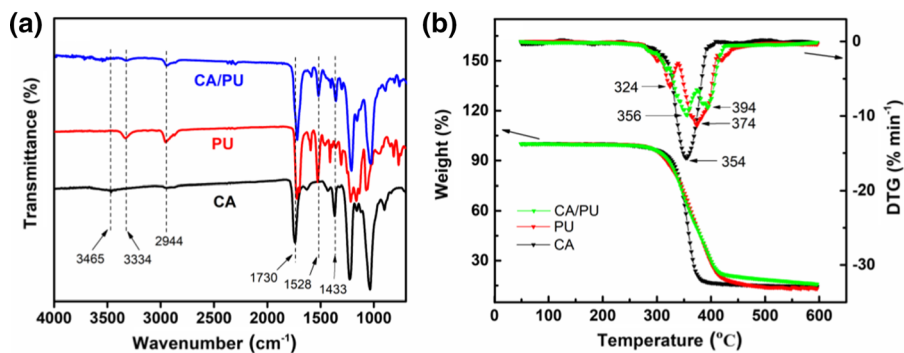


Fig. 2 a FTIR and b TG and DTG curves of CA, PU and CA/PU nanofiber membranes

peaks of PU (Riaz et al. 2016; Yin et al. 2018; Tan et al. 2015). The absorption peak at 3465 cm^{-1} is the stretching vibration peak of O–H, which belongs to the characteristic peak of CA (Zhang et al. 2021). After PU and CA were blended, the strength of the stretching and bending vibration peak of N–H decreased, while the stretching vibration peak of O–H moved to the high wave number direction, which may be caused by the formation of hydrogen bond between the hydroxyl group of CA and the amino group of PU.

In industrial applications, it is necessary for the membrane to have good thermal stability. The thermal behavior of nanofiber membrane was evaluated by thermogravimetric (TG) analysis. As shown in Fig. 2b, the thermal decomposition of pure CA nanofiber membrane occurs between 282 and 384 °C, and the maximum decomposition temperature is 354 °C. This weight loss of CA membrane material comes from the degradation of CA chain, that is, the pyrolysis of CA skeleton, followed by the deacetylation of CA (Arthanareeswaran et al. 2004; Lucena et al. 2003). The thermal decomposition process of pure PU nanofiber membrane is complex. The initial decomposition temperature is 280 °C, and there are two maximum decomposition temperatures, 324 and 374 °C respectively. Because the aromatic ring system has a destabilizing effect on the carbamate bond, the hard segment (MDI) of PU begins to degrade first, and the degradation rate is the highest at 324 °C. After that, the soft segment (PEG) of PU is decomposed, and the degradation rate reaches the maximum at 374 °C (Zavastin et al. 2010; Coutinho et al. 2003; Petrović et al. 1994). After the blending of PU and CA, the two maximum thermal decomposition temperatures of CA/PU nanofiber membrane are significantly higher

than those of pure PU membrane, which are 356 and 394 °C respectively. This is because the carbamate bond of PU is easier to degrade than CA chain, which has a greater impact on the thermal stability of the blended nanofiber membrane. The positive shift of DTG peak and the increase of residue at 450 °C also show that the thermal stability of CA/PU blend nanofiber membrane has been improved (Riaz et al. 2016; Iqhrammullah et al. 2020).

Membrane morphology

Figure 3a, b and c are SEM photos of the surfaces of CA, CA/PU and PU nanofiber membranes, respectively. It can be seen from the photos that there are obvious differences in the morphology of nanofibers constituting CA, CA/PU and PU membranes. The nanofiber diameter of PU membrane is fine and the number of fibers per unit area is large (Fig. 3c), while the nanofiber diameter of CA/PU membrane is coarse and uniform (Fig. 3b). The diameter distribution ranges of nanofibers of CA, CA/PU and PU membranes are 106–432 nm, 215–542 nm and 77–184 nm respectively, and the average diameters are 243 ± 99 nm, 351 ± 87 nm and 124 ± 26 nm separately (Fig. S3). There is adhesion between the nanofibers of PU membrane, which may be related to the high boiling point of DMAc solvent used in electrospinning. The volatilization speed of solvent with high boiling point is slow, resulting in adhesion at the fiber contact point (Tang et al. 2008). The interaction between polymer molecular chains is one of the main factors affecting the average diameter of electrospun nanofibers. After CA and PU are blended, due to the easy formation of hydrogen bonds between

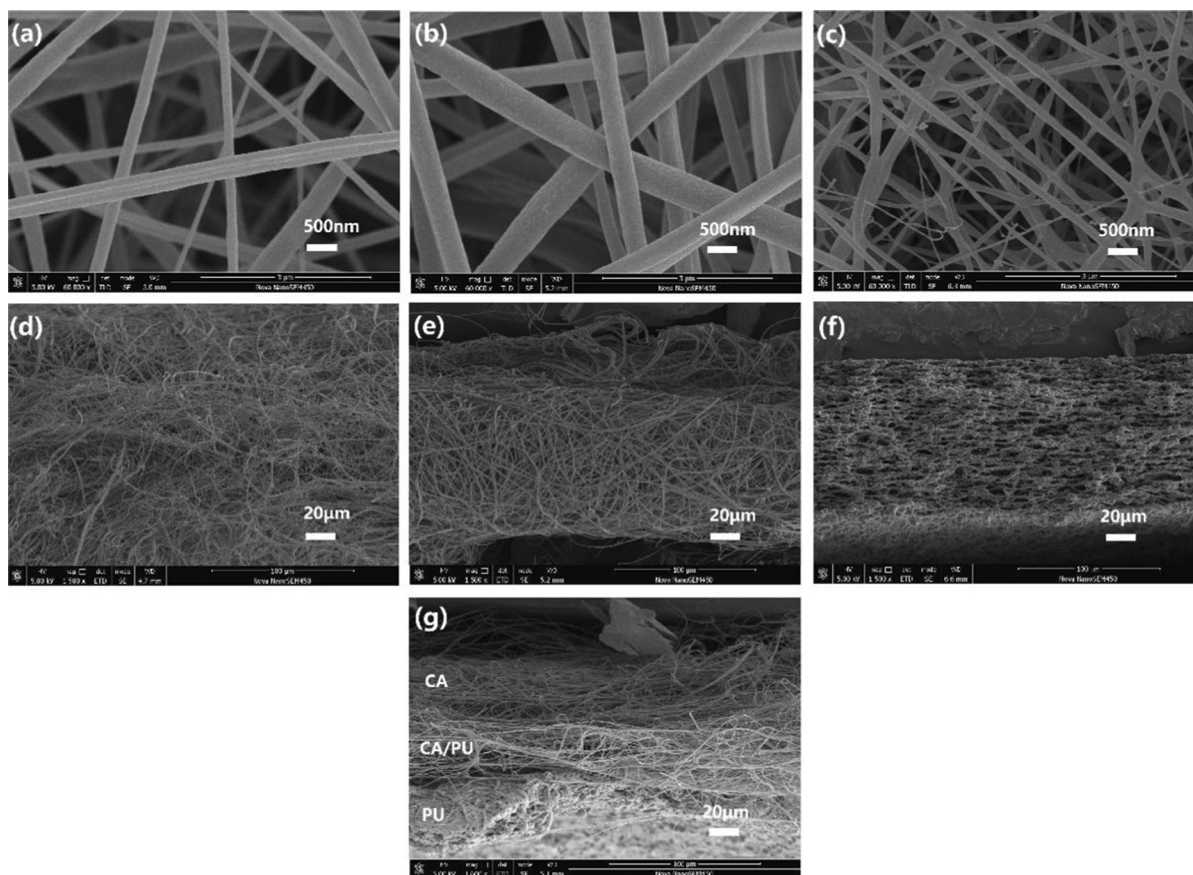


Fig. 3 SEM images of the surfaces of **a** CA, **b** CA/PU and **c** PU membranes, and SEM images of brittle fracture surfaces of **d** CA, **e** CA/PU, **f** PU and **g** PU-(CA/PU)-CA membranes

hydroxyl, carbonyl and amide groups of CA and PU, the interaction between molecular chains is enhanced, and the stress relaxation time of CA/PU blend polymer solution is increased, which leads to the formation of large-diameter fibers during electrospinning (Fong et al. 1999; Yao et al. 2008).

Figure 3d, e and f are SEM photos of brittle fracture surfaces of CA, CA/PU and PU nanofiber membranes, respectively. Obvious nanofibers can be seen on the fracture surfaces of CA and CA/PU membranes separately, while the fracture surface of PU membrane shows a honeycomb structure composed of adhesive bead fibers. This is because when electrospinning at low concentration, the chain entanglement makes the jet unstable, and the diameter of the jet shrinks under the action of surface tension, making the solution form bead fiber or bead (Cui et al. 2020). Figure 3g is a brittle fracture surface photo of PU-(CA/PU)-CA sandwich nanofiber Janus membrane. From Fig. 3g,

three-layer membrane structure can be identified. The upper layer is CA nanofiber membrane, the middle layer is CA/PU blend nanofiber membrane, and the lower layer is PU nanofiber membrane.

Wettability of CA, CA/PU and PU nanofiber membranes

The wettability of membrane is usually characterized by the contact angle of liquid on the membrane surface. The test results of contact angle are shown in Fig. 4a. The water contact angle (WCA) of CA nanofiber membrane is $64.3 \pm 5^\circ$, which may be caused by the hydrophilicity of ester groups and incompletely esterified hydroxyl groups of CA molecular chain (Zhang et al. 2021). The WCA of PU nanofiber membrane is $123.8 \pm 3^\circ$, indicating that PU membrane is hydrophobic. The WCA of CA/PU blend nanofiber membrane is $88.7 \pm 6^\circ$, which can be

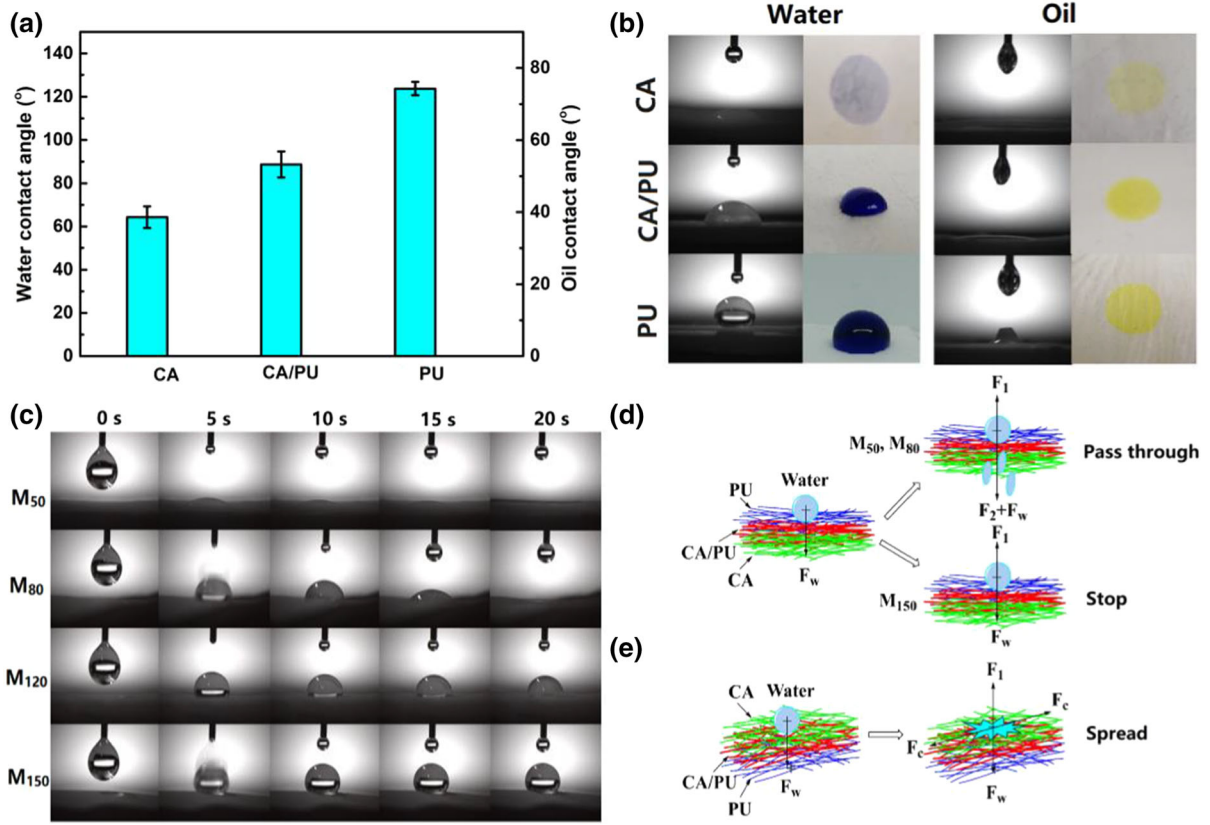


Fig. 4 **a** contact angle and **b** wettability test results of CA, CA/PU and PU nanofiber membrane, **c** wettability test of PU-(CA/PU)-CA nanofiber membrane with different thickness, **d** force

understood that CA/PU membrane is also hydrophilic, but the hydrophilicity is not as strong as CA membrane. The oil contact angle (OCA) test results of CA, CA/PU and PU nanofiber membranes are all 0°, indicating that the three membranes are super lipophilic (Su et al. 2021; Qing et al. 2017).

In order to further understand the wettability of liquid on nanofiber membranes, water dyed blue and oil (cyclohexane) dyed yellow were dropped onto different nanofiber membranes, and the wetting process was recorded with a camera. Results as shown in Fig. 4b, both water and cyclohexane can spread and wet rapidly on the surface of CA nanofiber membrane. CA membrane shows good hydrophilicity and lipophilicity and less wetting time (t_{wb}). Cyclohexane can also spread and wet on the surface of PU membrane and CA/PU membrane, and the wetting time (t_{wr}) of cyclohexane on PU membrane is greater than wetting time (t_{wm}) on CA/PU membrane, both of

diagram of water droplets passing through and staying on PU-(CA/PU)-CA nanofiber membrane, and **e** force diagram of water droplets diffusing from CA side of PU-(CA/PU)-CA membrane

which are greater than that on CA membrane ($t_{wr} > t_{wm} > t_{wb}$). Water has a certain degree of wetting on the surface of CA/PU membrane, but not on the surface of PU membrane. The wettability test results show that the wettability of water to CA, CA/PU and PU nanofiber membranes is significantly different.

PU-(CA/PU)-CA Janus membrane with nanofiber transition sandwich structure is composed of hydrophobic PU nanofiber membrane (top layer), CA/PU blend nanofiber membrane (middle transition layer) and hydrophilic CA nanofiber membrane (bottom layer). The directional transmission of water from top layer to bottom layer can be realized by using the difference of wettability. The photos of water droplets passing through PU-(CA/PU)-CA membranes with different thicknesses are shown in Fig. 4c. Water droplets can quickly pass-through membranes M₅₀ and M₈₀ with thickness of 50 and 80 μm respectively.

This is because when the top hydrophobic layer (PU) is thin, under the action of gravity (F_w), water droplets can easily contact the transition layer (CA/PU) and hydrophilic bottom layer (CA) through the hydrophobic layer. The downward hydrophilic force (F_2) and F_w jointly overcome the upward hydrophobic force (F_1), so that water droplets can pass through PU-(CA/PU)-CA nanofiber membrane (Fig. 4d). With the increase of top layer thickness, the chance of water droplets contacting the transition layer and hydrophilic bottom layer decreases under the action of gravity. F_1 prevents water droplets from continuing to pass through PU-(CA/PU)-CA nanofiber membrane. When the membrane thickness is 150 μm (M_{150}), F_1 and F_w are balanced, and the water droplets stay on the top layer and cannot pass through the PU-(CA/PU)-CA nanofiber membrane (Fig. 4d). On the contrary, when water droplets penetrate from the CA side of PU-(CA/PU)-CA nanofiber membrane, they first contact with hydrophilic CA nanofiber membrane, and the water droplets will spread rapidly and diffuse into CA nanofiber membrane through capillary force (F_c). The hydrophobic force F_1 of PU layer will also prevent water droplets from further passing through PU-(CA/PU)-CA nanofiber membrane (Fig. 4e) (Wu et al. 2012). Therefore, PU-(CA/PU)-CA nanofiber membrane can realize the directional transmission of water from the top PU layer to the bottom CA layer.

Oil water separation capacity of membrane

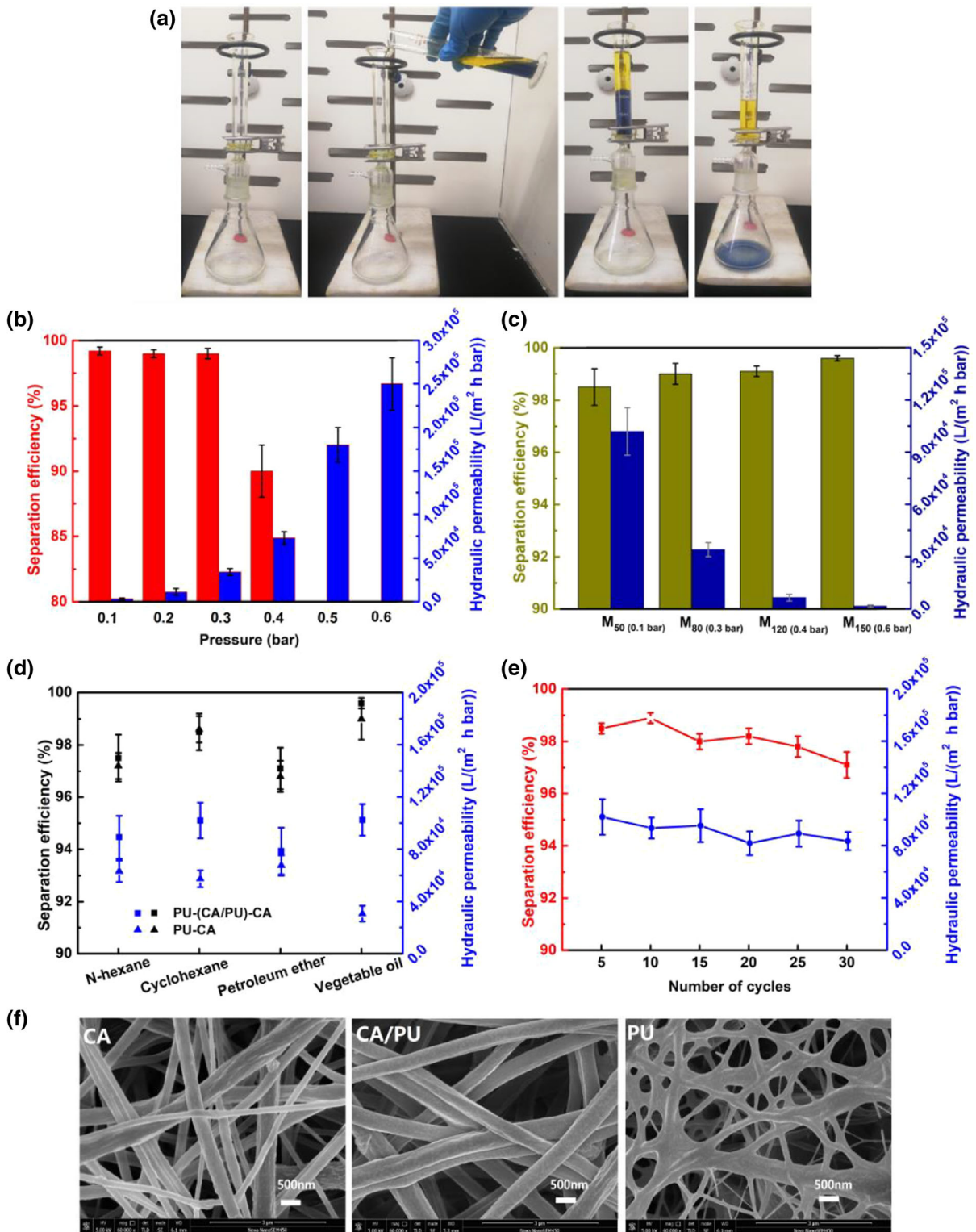
The wettability difference of PU-(CA/PU)-CA nanofiber membrane can be used for oil–water separation. As shown in Fig. 5a, methyl blue (blue) and 4-aminoazobenzene (yellow) were dissolved in water and oil (cyclohexane) respectively for dyeing, then the blue water and yellow oil were mixed, and then the oil–water mixture was poured into a separator equipped with PU-(CA/PU)-CA nanofiber membrane. When the oil–water mixture contacts the hydrophobic top layer of the membrane, the water in the lower layer of the mixture flows into the flask through the PU-(CA/PU)-CA nanofiber membrane driven by the transmembrane pressure, but the oil is blocked on the membrane to realize the oil–water separation (Video S1).

As an effective oil–water separation material, two important conditions must be met, namely, high separation flux and high separation efficiency (Zhang, et al. 2019a, b; Su et al. 2021). Therefore, we studied

the relationship between transmembrane pressure (P_t), membrane thickness and hydraulic permeability (L_p) and oil–water separation efficiency (E_s). Figure 5b shows the relationship between E_s , L_p and P_t of membrane M_{80} . It can be seen from Fig. 5b that when P_t is small, the E_s of membrane is very high ($\geq 99\%$), but L_p is small. When P_t reaches 0.3 bar, E_s remains above 99%, while L_p increases to $3.4 \pm 0.4 \times 10^4 \text{ L}/(\text{m}^2 \text{ h bar})$. With the further rise of P_t , L_p gradually increases, but the E_s of the membrane decreases sharply. When P_t reaches 0.5 bar, E_s is 0%, and the membrane loses the ability of oil–water separation. This is because large P_t enables the oil phase to pass through the nanofiber membrane, which makes the membrane lose the function of oil–water separation. Therefore, appropriate P_t is the key to ensure high E_s and high L_p of the membrane. In view of this, we selected 0.3 bar as the P_t for membrane M_{80} .

Using the same method, the P_t used for membranes M_{50} , M_{120} and M_{150} were determined to be 0.1, 0.4 and 0.6 bar respectively. Membranes with different thicknesses correspond to different P_t , and the greater the thickness of the membrane, the higher the corresponding P_t . The E_s and L_p of membranes with different thicknesses under different P_t are shown in Fig. 5c. As can be seen from Fig. 5c, the E_s of membranes is higher, more than 98.5%, and the greater the membrane thickness, the higher the E_s . When the membrane thickness is 150 μm (M_{150}), the E_s increases to $99.5 \pm 0.1\%$. L_p decreases significantly with the increase of membrane thickness. When the membrane thickness is 150 μm , L_p is only $0.15 \pm 0.06 \times 10^4 \text{ L}/(\text{m}^2 \text{ h bar})$. Thus, for the sake of achieving high L_p and high E_s simultaneously, the membrane thickness should be reduced as much as possible while ensuring that E_s meets the requirements. Here, we selected the membrane with thickness of 50 μm (M_{50}) for follow-up test.

In order to further evaluate the oil–water separation ability of PU-(CA/PU)-CA nanofiber membrane, different kinds of oil/water mixtures were selected for separation experiments and compared with 50 μm thick PU-CA nanofiber membrane without transition interlayer. As shown in Fig. 5d, PU-(CA/PU)-CA nanofiber membrane M_{50} can successfully separate oil/water mixtures such as n-hexane/water, cyclohexane/water, petroleum ether/water and vegetable oil/water, and both E_s and L_p are high. The E_s and L_p of petroleum ether/water with poor oil–water separation



◀ **Fig. 5** **a** photos of oil–water separation experiment of nanofiber membrane, **b** relationship diagram of E_s , L_p and P_f of membrane M_{80} , **c** relationship diagram of E_s , L_p and PU-(CA/PU)-CA membrane thickness under different P_f , **d** E_s and L_p diagram of PU-(CA/PU)-CA membrane and PU-CA membrane for different oil–water mixtures, **e** E_s and L_p diagram of PU-(CA/PU)-CA membrane under different number of cycles, and **f** SEM images of the surfaces of CA, CA/PU and PU membrane after 30 oil–water separation cycles

also reaches $97.1 \pm 0.8\%$ and $7.85 \pm 1.78 \times 10^4$ L/(m² h bar), respectively. The E_s of PU-CA nanofiber membrane for different kinds of oil–water mixtures is equivalent to that of PU-(CA/PU)-CA membrane, while L_p is lower than that of PU-(CA/PU)-CA membrane, which may be due to the PU layer thickness (25 μm) of PU-CA membrane is greater than that (20 μm) of PU-(CA/PU)-CA membrane (Zhang et al. 2019a, b). The molecular weight cut-off (MWCO) experiment shows that the MWCO of PU-(CA/PU)-CA membrane is 550 kDa, while the MWCO of PU-CA membrane is close to 1000 kDa, and the macromolecular rejection ability of PU-(CA/PU)-CA membrane is stronger than that of PU-CA membrane (Fig. S4) (Arkhangelsky et al. 2012; Chen et al. 2021; Yao et al. 2021).

In addition, the reusability and cyclic separation efficiency of PU-(CA/PU)-CA nanofiber membrane were also tested with cyclohexane/water mixture. As shown in Fig. 5e, after 30 cycles of separation experiments, PU-(CA/PU)-CA nanofiber membrane M_{50} still maintains high E_s ($97.2 \pm 0.5\%$) and L_p ($8.34 \pm 0.7 \times 10^4$ L/(m² h bar)). Compared with the initial E_s ($98.5 \pm 0.2\%$) and L_p ($10.19 \pm 1.37 \times 10^4$ L/(m² h bar)) of the membrane M_{50} , the E_s and L_p of the membrane M_{50} after 30 cycles of use decreases, which may be because the lipophilicity of the top PU nanofiber membrane is easy to make the cyclohexane adhere to the membrane surface, and the dissolution and corrosion of cyclohexane on the PU nanofiber membrane reduces the E_s and L_p of the membrane (Pan et al. 2017). The cyclic separation experiment shows that PU-(CA/PU)-CA nanofiber membrane has high reusability.

Figure 5f is SEM photos of CA, CA/PU and PU membrane surfaces after 30 oil–water separation cycle experiments, respectively. It can be seen from Fig. 5f that the nanofibers of the repeatedly used PU membrane swell and adhere, which may be caused by the

lipophilic PU membrane adsorbing cyclohexane, and cyclohexane partially dissolving the PU nanofibers. The nanofibers of CA membrane and CA/PU blend membrane basically maintain their original morphology after repeated recycling, which may be because the hydrophilicity of CA membrane and CA/PU blend membrane forms a protective water layer on the membrane surface to avoid oil fouling (Lv et al. 2017; De Guzman et al. 2021). This also indicates that the antifouling performance of CA/PU nanofiber membrane is improved after CA and PU are blended.

Tensile test of membrane

In order to understand the influence of the composition and structure of nanofiber membrane on the mechanical properties of the membrane, tensile tests were carried out on pure PU membrane, pure CA membrane, CA/PU blend membrane, PU-CA bilayer Janus membrane without interlayer and PU-(CA/PU)-CA transition interlayer Janus membrane. As shown in Fig. 6, the tensile strength (T_s) and elongation at break (E_b) of pure PU nanofiber membrane are the largest, which are 3.59 ± 0.38 MPa and $135.51 \pm 9.34\%$, respectively, while the T_s and E_b of pure CA nanofiber membrane are lower, which are 0.89 ± 0.17 MPa and $8.99 \pm 1.46\%$, separately. After CA and PU are blended, the T_s and E_b of CA/PU blend nanofiber membrane are more than twice that of pure CA nanofiber membrane, which are 1.93 ± 0.04 MPa and $19.93 \pm 1.23\%$ respectively. It shows that CA/PU blend nanofiber membrane has the characteristics of high strength of PU membrane and low elongation at break of CA membrane. It can also be seen from Fig. 6

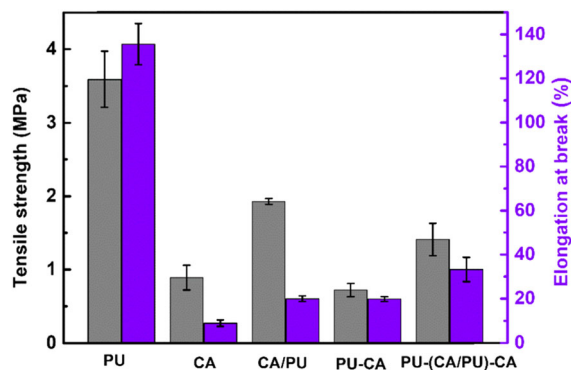


Fig. 6 Tensile strength and elongation at break of nanofiber membranes with different composition and structure

that the T_s and E_b of PU-(CA/PU)-CA membrane with CA/PU blend nanofiber as transition interlayer are 1.41 ± 0.22 MPa and $33.22 \pm 5.5\%$, which are 95.8% and 67.9% higher than that of PU-CA membrane with double-layer structure, separately. This indicates that PU-(CA/PU)-CA transition sandwich Janus membrane has better strength and toughness than PU-CA bilayer Janus membrane.

Conclusion

PU-(CA/PU)-CA nanofiber Janus membranes with CA/PU blend nanofibers as transition interlayer were constructed by sequential electrospinning. CA/PU transition interlayer improves the thermal stability of the membrane and the interfacial compatibility of nanofiber membranes with different properties, and enhances the mechanical properties of PU-(CA/PU)-CA membrane. The T_s of PU-(CA/PU)-CA nanofiber membrane is 95.8% higher than that of PU-CA double-layer nanofiber membrane. PU-(CA/PU)-CA nanofiber membrane has high permeability and selective separation ability, and the L_p and E_s of the membrane with a thickness of 80 μm reach $3.4 \pm 0.4 \times 10^4$ L/(m² h bar) and $99 \pm 0.4\%$ respectively. PU-(CA/PU)-CA nanofiber membrane also has good antifouling performance and reusability. CA/PU transition interlayer improves the performance of PU-(CA/PU)-CA nanofiber Janus membrane, and shows its application prospect in the field of separation and purification.

Acknowledgments This work was sponsored by the National Natural Science Foundation of China (Nos. 22075189, 51803128, 52073186), Strategic Cooperation between Sichuan University and Yibin City (No. 2019CDYB-30), Strategic Project of Zi Gong Science & Technology Bureau (Nos. 2019CDZG-S15, 2020CDZG-15), and Funding of Engineering Characteristic Team, Sichuan University (2020SCUNG122).

Authors' contributions Yong Zhang: Conceptualization, Data Curation, Writing—Original Draft, Funding acquisition. Mei Yang: Formal analysis. Yuan Zhou: Investigation, Data Curation. Anrong Yao: Investigation, Data Curation, Writing—Original Draft. Yanting Han: Data Curation. Yidong Shi: Project administration. Fei Cheng: Resources. Mi Zhou: Resources. Puxin Zhu: Supervision. Lin Tan: Conceptualization, Methodology, Project administration, Funding acquisition.

Funding This work was sponsored by the National Natural Science Foundation of China (Nos. 22075189, 51803128, 52073186), Strategic Cooperation between Sichuan University and Yibin City (No. 2019CDYB-30), Strategic Project of Zi Gong Science & Technology Bureau (Nos. 2019CDZG-S15, 2020CDZG-15), and Funding of Engineering Characteristic Team, Sichuan University (2020SCUNG122).

Declaration

Conflicts of interest All authors declare that they have no conflict of interest.

Consent for publication Yes, my co-authors and I would like to publish.

References

- Arkhangelsky E, Duek A, Gitis V (2012) Maximal pore size in UF membranes. *J Membr Sci* 394–395:89–97
- Arthanareeswaran G, Thanikaivelan P, Srinivasn K, Mohan D, Rajendran M (2004) Synthesis, characterization and thermal studies on cellulose acetate membranes with additive. *Eur Polymer J* 40:2153–2159
- Bates C, Ileana I, Loranger É, Mathew AP, Chabot B (2021) Cellulose reinforced electrospun chitosan nanofibers bio-based composite sorbent for water treatment applications. *Cellul* 28:4865–4885
- Chen Y, Kim S, Cohen Y (2021) Tuning the hydraulic permeability and molecular weight cutoff (MWCO) of surface nano-structured ultrafiltration membranes. *J Membr Sci* 629:119180
- Coutinho FMB, Delpech MC, Alves TL, Ferreira AA (2003) Degradation profiles of cast films of polyurethane and poly(urethane-urea) aqueous dispersions based on hydroxy-terminated polybutadiene and different diisocyanates. *Polym Degrad Stab* 81:19–27
- Cui J, Li F, Wang Y, Zhang Q, Ma W, Huang C (2020) Electrospun nanofiber membranes for wastewater treatment applications. *Sep Purif Technol* 250:117116
- Dai R, Li J, Wang Z (2020) Constructing interlayer to tailor structure and performance of thin-film composite polyamide membranes: a review. *Adv Colloid Interface Sci* 282:102204
- Guzman D, Reyes M, Chester KA, Andra MB, Ang MY, Gian VC, Dizon AR, Caparanga S-HH, Lee K-R (2021) Increased performance and antifouling of mixed-matrix membranes of cellulose acetate with hydrophilic nanoparticles of polydopamine-sulfobetaine methacrylate for oil-water separation. *J Membr Sci* 620:118881
- Fong H, Chun I, Reneker DH (1999) Beaded nanofibers formed during electrospinning. *Polymer* 40:4585–4592
- Hu L, Gao S, Zhu Y, Zhang F, Jiang L, Jin J (2015) An ultrathin bilayer membrane with asymmetric wettability for pressure responsive oil/water emulsion separation. *J Mater Chem A* 3:23477–23482

- Iqhrammullah, M., Marlina Marlina, H. P. S. Abdul Khalil, K. H. Kurniawan, H. Suyanto, R. Hedwig, I. Karnadi, N. G. Olaiya, C. K. Abdullah, and S. N. Abdulmajid. 2020. 'Characterization and Performance Evaluation of Cellulose Acetate-Polyurethane Film for Lead II Ion Removal.', *Polymers*, 12.
- Jiang L, Li Ke, Yang H, Liu X, Li W, Weilin Xu, Deng Bo (2020) Improving mechanical properties of electrospun cellulose acetate nanofiber membranes by cellulose nanocrystals with and without polyvinylpyrrolidone. *Cellul* 27:955–967
- Ju X, Jin-Peng L, Zhao L-L, Tian-Dan L, Cao X-L, Jia T-Z, Wang Y-C, Sun S-P (2021) Electrospun transition layer that enhances the structure and performance of thin-film nanofibrous composite membranes. *J Membr Sci* 620:118927
- Li H, Wang X, He Y, Peng L (2019) Facile preparation of fluorine-free superhydrophobic/superoleophilic paper via layer-by-layer deposition for self-cleaning and oil/water separation. *Cellul* 26:2055–2074
- Liu H, Huang J, Li F, Chen Z, Zhang K-Q, Al-Deyab SS, Lai Y (2017) Multifunctional superamphiphobic fabrics with asymmetric wettability for one-way fluid transport and templated patterning. *Cellul* 24:1129–1141
- Liu Y, Qu R, Zhang W, Li X, Wei Y, Feng L (2019) Lotus- and Mussel-Inspired PDA–PET/PTFE Janus Membrane: Toward Integrated Separation of Light and Heavy Oils from Water. *ACS Appl Mater Interfaces* 11:20545–20556
- Liu Y, Zhan B, Zhang K, Kaya C, Stegmaier T, Han Z, Ren L (2018) On-demand oil/water separation of 3D Fe foam by controllable wettability. *Chem Eng J* 331:278–289
- Lucena M, da Conceição C, Ana EV, de Alencar S, Mazzeto E, de Soares S A. (2003) The effect of additives on the thermal degradation of cellulose acetate. *Polym Degrad Stab* 80:149–155
- Lv J, Zhang G, Zhang H, Yang F (2017) Exploration of permeability and antifouling performance on modified cellulose acetate ultrafiltration membrane with cellulose nanocrystals. *Carbohydr Polym* 174:190–199
- Nosar MN, Salehi M, Ghorbani S, Beiranvand SP, Goodarzi A, Azami M (2016) Characterization of wet-electrospun cellulose acetate based 3-dimensional scaffolds for skin tissue engineering applications: influence of cellulose acetate concentration. *Cellul* 23:3239–3248
- Pan J, Xiao C, Huang Q, Liu H, Zhang T (2017) ECTFE hybrid porous membrane with hierarchical micro/nano-structural surface for efficient oil/water separation. *J Membr Sci* 524:623–630
- Petrović ZS, Zavargo Z, Flynn JH, Macknight WJ (1994) Thermal degradation of segmented polyurethanes. *J Appl Polym Sci* 51:1087–1095
- Qing W, Shi X, Deng Y, Zhang W, Wang J, Tang CY (2017) Robust superhydrophobic-superoleophilic polytetrafluoroethylene nanofibrous membrane for oil/water separation. *J Membr Sci* 540:354–361
- Riaz T, Ahmad A, Saleemi S, Adrees M, Jamshed F, Hai AM, Jamil T (2016) Synthesis and characterization of polyurethane-cellulose acetate blend membrane for chromium (VI) removal. *Carbohydr Polym* 153:582–591
- Song H-M, Chen C, Shui X-X, Yang H, Zhu L-J, Zeng Z-X, Xue Q-J (2019) Asymmetric Janus membranes based on in situ mussel-inspired chemistry for efficient oil/water separation. *J Membr Sci* 573:126–134
- Su R, Li S, Wanlin W, Song C, Liu G, Yang Y (2021) Recent progress in electrospun nanofibrous membranes for oil/water separation. *Sep Purif Technol* 256:117790
- Tan L, Jinlian Hu, Huang H, Han J, Huawen Hu (2015) Study of multi-functional electrospun composite nanofibrous mats for smart wound healing. *Int J Biol Macromol* 79:469–476
- Tang C, Chen P, Liu H (2008) Cocontinuous cellulose acetate/polyurethane composite nanofiber fabricated through electrospinning. *Polym Eng Sci* 48:1296–1303
- Wang X, Jianyong Yu, Sun G, Ding B (2016a) Electrospun nanofibrous materials: a versatile medium for effective oil/water separation. *Mater Today* 19:403–414
- Wang Z, Wang Yu, Liu G (2016b) Rapid and efficient separation of oil from oil-in-water emulsions using a janus cotton fabric. *Angew Chem Int Ed* 55:1291–1294
- Wu J, Wang Nü, Wang Li, Dong H, Zhao Y, Jiang L (2012) Unidirectional water-penetration composite fibrous film via electrospinning. *Soft Matter* 8:5996–5999
- Xie A, Cui J, Liu Y, Xue C, Wang Y, Dai J (2021) Preparation of Janus membrane based on biomimetic polydopamine interface regulation and superhydrophobic attapulgite spraying for on-demand oil-water emulsion separation. *J Membr Sci* 627:119242
- Yang H-C, Hou J, Chen V, Zhi-Kang Xu (2016) Janus membranes: exploring duality for advanced separation. *Angew Chem Int Ed* 55:13398–13407
- Yao A, Yan Y, Tan L, Shi Y, Zhou M, Zhang Y, Zhu P, Huang S (2021) Improvement of filtration and antifouling performance of cellulose acetate membrane reinforced by dopamine modified cellulose nanocrystals. *J Membr Sci* 637:119621
- Yao C, Xinsong Li KG, Neoh ZS, Kang ET (2008) Surface modification and antibacterial activity of electrospun polyurethane fibrous membranes with quaternary ammonium moieties. *J Membr Sci* 320:259–267
- Yin X, Wen Y, Li Y, Liu P, Li Z, Shi Y, Lan J, Guo R, and Tan L. 2018. 'Facile Fabrication of Sandwich Structural Membrane With a Hydrogel Nanofibrous Mat as Inner Layer for Wound Dressing Application', *Frontiers in Chemistry*, 6.
- Zavastin D, Cretescu I, Bezdadea M, Bourceanu M, Drăgan M, Lisa G, Mangalagiu I, Vasić V, Savić J (2010) Preparation, characterization and applicability of cellulose acetate-polyurethane blend membrane in separation techniques. *Colloids Surf, A* 370:120–128
- Zhang J, Ge J, Si Y, Zhang F, Jianyong Yu, Liu L, Ding B (2019a) Taro leaf-inspired and superwetable nanonet-covered nanofibrous membranes for high-efficiency oil purification. *Nanoscale Horizons* 4:1174–1184
- Zhang J, Zhang F, Song J, Liu L, Si Y, Jianyong Yu, Ding B (2019b) Electrospun flexible nanofibrous membranes for oil/water separation. *J Mater Chem A* 7:20075–20102
- Zhang J, Yang Y, Zhang Z, Wang P, Wang X (2014) Biomimetic multifunctional nanochannels based on the asymmetric wettability of heterogeneous nanowire membranes. *Adv Mater* 26:1071–1075
- Zhang YQ, Yang XB, Wang ZX, Long J, Shao Lu (2017) Designing multifunctional 3D magnetic foam for effective insoluble oil separation and rapid selective dye removal for

use in wastewater remediation. *J Mater Chem A* 5:7316–7325

Zhang Y, Tan L, Yao A, Tan P, Guo R, Zhou Mi, Zhu P, Huang S, Yunheng Wu (2021) Improvement of filtration performance of polyvinyl chloride/cellulose acetate blend membrane via acid hydrolysis. *J Appl Polym Sci* 138:50312

Publisher's Note Springer Nature remains neutral with regard to jurisdictional claims in published maps and institutional affiliations.